Cerebellothalamocortical pathway abnormalities in torsinA DYT1 knock-in mice

Aziz M. Ulug[a,b], An Vo[a], Miklos Argyelan[a], Lauren Tanabe[c], Wynne K. Schiffer[a], Stephen Dewey[a], William T. Dauer[c], and David Eidelberg[a,1]

[a]Center for Neurosciences, The Feinstein Institute for Medical Research, Manhasset, NY 11030; [b]Department of Radiology, Albert Einstein College of Medicine, Bronx, NY 10461; and [c]Departments of Neurology and Cell and Developmental Biology, University of Michigan Medical School, Ann Arbor, MI 48109

Edited* by Joanna S. Fowler, Brookhaven National Laboratory, Upton, NY, and approved February 16, 2011 (received for review November 12, 2010)

The factors that determine symptom penetrance in inherited disease are poorly understood. Increasingly, magnetic resonance diffusion tensor imaging (DTI) and PET are used to separate alterations in brain structure and function that are linked to disease symptomatology from those linked to gene carrier status. One example is DYT1 dystonia, a dominantly inherited movement disorder characterized by sustained muscle contractions, postures, and/or involuntary movements. This form of dystonia is caused by a 3-bp deletion (i.e., ΔE) in the *TOR1A* gene that encodes torsinA. Carriers of the DYT1 dystonia mutation, even if clinically nonpenetrant, exhibit abnormalities in cerebellothalamocortical (CbTC) motor pathways. However, observations in human gene carriers may be confounded by variability in genetic background and age. To address this problem, we implemented a unique multimodal imaging strategy in a congenic line of DYT1 mutant mice that contain the ΔE mutation in the endogenous mouse torsinA allele (i.e., DYT1 knock-in). Heterozygous knock-in mice and littermate controls underwent microPET followed by ex vivo high-field DTI and tractographic analysis. Mutant mice, which do not display abnormal movements, exhibited significant CbTC tract changes as well as abnormalities in brainstem regions linking cerebellar and basal ganglia motor circuits highly similar to those identified in human nonmanifesting gene carriers. Moreover, metabolic activity in the sensorimotor cortex of these animals was closely correlated with individual measures of CbTC pathway integrity. These findings further link a selective brain circuit abnormality to gene carrier status and demonstrate that DYT1 mutant torsinA has similar effects in mice and humans.

connectivity | regional metabolism | brain networks

In recent years, advanced imaging technologies such as PET and magnetic resonance diffusion tensor imaging (DTI) have provided unique information regarding the impact of specific genetic mutations on brain structure and function. However, to control for variability in genetic background and additional confounders such as age and sex, many more mutation carriers (and control subjects) are required than can conveniently be scanned, even in a multicenter design. Human imaging studies may also suffer from relatively low spatial resolution and sensitivity. These considerations motivated the current study in which high field magnetic resonance DTI was performed ex vivo in an experimental genetic model of a brain disorder.

Primary dystonia is a childhood-onset neurological illness characterized by disabling abnormal involuntary movements without consistent brain lesions on routine structural brain imaging or at postmortem analysis (1). This disorder is associated with several genotypes (2). DYT1 dystonia, the most common inherited form of the disease, is caused by a dominantly inherited 3-bp in-frame deletion in the *TOR1A* gene that removes a single glutamic acid (ΔE) from the torsinA protein (3). This low-prevalence mutation (approximately 1 in 30,000) (4) is also incompletely penetrant, causing dystonic symptoms in only 30% to 40% of gene carriers (5).

Functional imaging studies comparing DYT1 mutation carriers with and without clinical manifestations to control subjects have contributed to the current understanding of disease mechanisms (6, 7). DYT1 gene carriers exhibit abnormal increases in regional metabolic activity in the cerebellum, putamen/globus pallidus, and supplementary motor cortex, irrespective of clinical penetrance (8, 9). Indeed, these metabolic changes are present during sleep when no involuntary movements are present, suggesting an association with genotype rather than phenotype (8, 10, 11). Magnetic resonance DTI shows white matter abnormalities in dystonia gene carriers (12, 13), and tractographic analysis of these abnormalities has associated these changes with reduced integrity of cerebellothalamocortical (CbTC) motor pathways (6), which modulate the excitability and synaptic plasticity of the sensorimotor cortex (14). Irrespective of clinical penetrance, DYT1 carriers exhibited reduced connectivity in the proximal cerebellothalamic segment of this pathway. By contrast, nonmanifesting carriers were distinguished by additional tract deficits involving the distal thalamocortical segment of this projection system. The presence of tandem tract changes in these mutation carriers raises the possibility that the additional abnormality prevents clinical manifestations by interrupting the transmission of aberrant cerebellar output signals to motor cortex (6, 15).

In this study we use a unique multimodal animal imaging approach to control for the potential confounds described earlier in relation to human mutation carriers. Congenic C57Bl6/J DYT1 knock-in mice heterozygous for the ΔE mutation in the *TOR1A* gene (*Tor1a*$^{\Delta E/+}$) (16) and littermate controls (*Tor1a*$^{+/+}$) were scanned ex vivo with high field MR DTI followed by tractographic analysis. Because they are fully congenic, *Tor1a*$^{\Delta E/+}$ and *Tor1a*$^{+/+}$ mice are 99.9% genetically identical, enabling us to isolate and study the CNS effects of the ΔE mutation. Significant microstructural abnormalities were identified in the CbTC pathways of the mutant animals. The relationship of these tract changes to regional brain function was assessed by correlation with measurements of cerebral metabolism acquired in vivo with [^{18}F]fluorodeoxyglucose (FDG) microPET. These studies allowed for the direct assessment of the effect of the DYT1 mutation on the structure and function of CbTC motor pathways.

Results

Several discrete regions with abnormal white matter microstructure (Fig. 1*A*) were identified in the *Tor1a*$^{\Delta E/+}$ mice (Table 1). Significant reductions in fractional anisotropy (FA), a DTI index of axonal integrity and coherence, were present in the mutant animals relative to controls ($P < 0.0001$, Student t tests). These abnormalities were localized to the right superior cerebellar tract (cluster 1), the white matter subjacent to the right primary sensorimotor cortex (cluster 2), and the left caudate/

Author contributions: A.M.U., W.T.D., and D.E. designed research; A.M.U., A.V., and L.T. performed research; A.M.U., A.V., M.A., W.K.S., S.D., and D.E. analyzed data; and A.M.U. and D.E. wrote the paper.

The authors declare no conflict of interest.

*This Direct Submission article had a prearranged editor.

[1]To whom correspondence should be addressed. E-mail: david1@nshs.edu.

www.pnas.org/cgi/doi/10.1073/pnas.1016445108

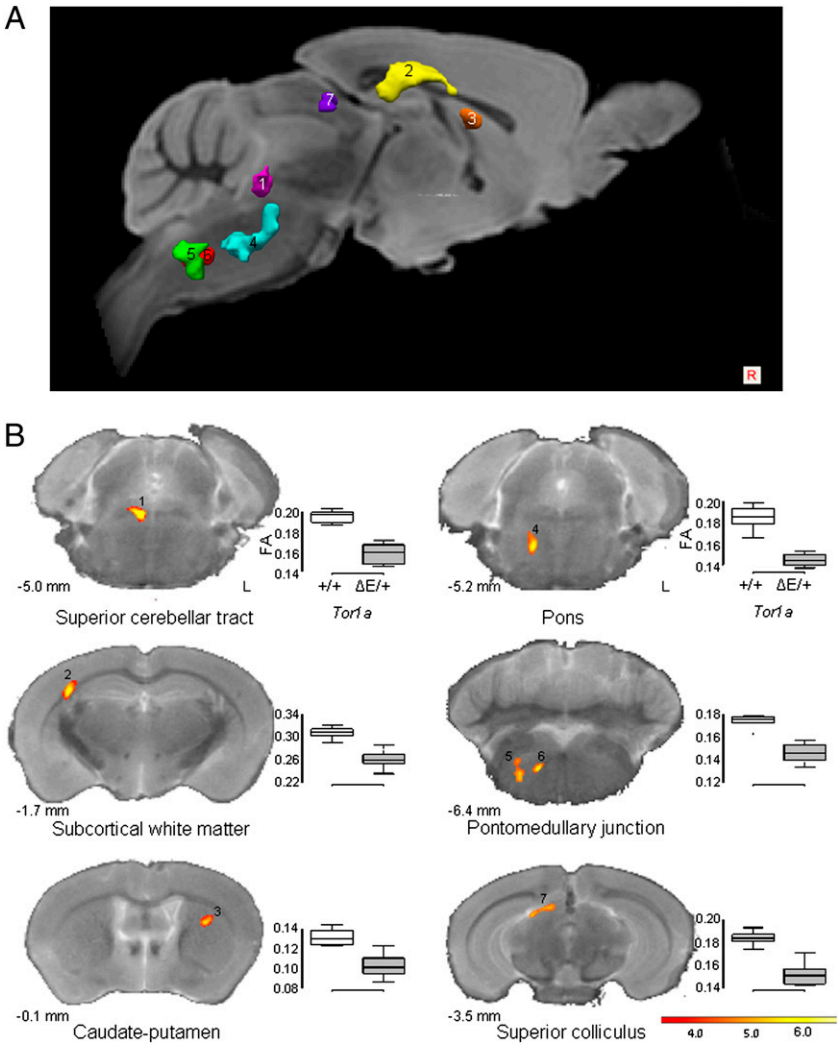

Fig. 1. Regions with abnormal microstructure in *Tor1a*$^{\Delta E/+}$ mice. (*A*) Three-dimensional display of regions with abnormal white matter microstructure in the mutant animals (Table 1). Significant reductions ($P < 0.0001$, Student *t* test) in FA were present in the following brain areas: superior cerebellar tract (marked by "1"), subcortical white matter in the primary sensory and motor regions ("2"), caudate/putamen ("3"), pons in the vicinity of the reticular nuclei ("4"), lateral pontomedullary junction ("5"), medial pontomedullary junction ("6"), and white matter adjacent to the superior colliculus ("7"). (*B*) Two-dimensional displays of these clusters overlaid on a standard mouse MRI template (37). The color scale represents *t* values threshold at 3.9 corresponding to $P < 0.001$ (uncorrected). Individual cluster values for the mutant and for the control groups are represented by box-and-whisker plots. All group differences were highly significant ($P < 0.0001$).

putamen (cluster 3). Of note, the FA reductions observed in these regions were also significant ($P < 0.05$) in homologous areas on the opposite side of the brain. Each of these clusters was then used as a seed region for fiber tracking. In the control animals, group tractography revealed extensive anatomical connections between these regions and the ventral thalamus (Fig. 2*A*). In each of these pathways, fewer tracts were visualized in the mutant group (Fig. 2*B*). This observation was substantiated by the quantitative fiber counts that were conducted in the individual animals. These measurements in the mutant animals revealed reduced tract numbers relative to littermate controls ($P < 0.001$, Student *t* tests) in cerebellothalamic (−49%), thalamocortical (−55%), and thalamostriatal (−86%) projection pathways.

Several additional regions (Fig. 1*B*) were identified in the mutant animals that were associated with unilateral abnormalities in pathway microstructure (Table 1). Two areas of reduced FA ($P < 0.0001$) were present in the right pons, in the vicinity of the reticular nuclei (clusters 4 and 5). Tractographic analysis in the control animals disclosed that both these areas were connected to the cerebellum through the inferior peduncle (Fig. 2*C*). The mutant group exhibited fewer tracts in these pathways (Fig. 2*D*), with significant fiber count reductions in the *Tor1a*$^{\Delta E/+}$ animals in the rostral (−59%, $P = 0.003$) and caudal (−86%, $P < 0.001$) pontocerebellar pathways. Additional FA reductions in the mutant animals ($P < 0.0001$) were noted medially in the right caudal pons (cluster 6) and in the white matter adjacent to the right superior colliculus (cluster 7), without consistent tractographic correlates. No connections were discerned between basal ganglia structures and any of the significant clusters identified in the voxel-wise group comparison.

We next determined whether the pathway abnormalities identified in the *Tor1a*$^{\Delta E/+}$ mice were associated with discrete alterations in regional brain function analogous to those observed in human *DYT1* mutation carriers. Specifically, we examined the hypothesis that the changes in CbTC pathway microstructure seen in mutation carriers correlate with metabolic activity at downstream nodes of this network. FDG microPET disclosed a single brain region with abnormal glucose utilization in the *Tor1a*$^{\Delta E/+}$ mice (Table 1). This change (Fig. 3*A*) was localized to the superior cerebellar vermis (lobule VI) (17), with increased local metabolic activity in mutant relative to control animals ($P < 0.001$, Student *t* test).

We then examined the relationship between individual differences in CbTC tract integrity and resting metabolic activity in the mutant group. Given that all the *Tor1a*$^{\Delta E/+}$ mice exhibited proximal (cluster 1) as well as distal (cluster 2) tract abnormalities along this pathway, FA values from both these white matter regions were entered as covariates in a voxel-wise search for regions in which brain metabolism correlated with pathway microstructure. A significant structure–function correlation ($P < 0.0001$, multiple linear regression; Table 1) was identified in a

Table 1. Voxel-based comparison of pathway microstructure and regional metabolic activity in mutant versus control animals

Region	Coordinates*			Cluster Size†	Z_{max}	*P* Value
	x	y	z			
Regions with significant group differences in FA						
Mutant < Control						
1. Superior cerebellar tract	0.4	−5.0	−3.6	190	3.94	0.002‡
2. Subcortical white matter (sensorimotor)	2.9	−1.7	−1.5	682	4.20	<0.001‡
3. Caudate/putamen	−2.3	−0.1	−2.3	102	3.93	0.019‡
4. Pons	0.4	−5.5	−5.1	661	4.28	<0.001
5. Lateral pontomedullary junction	1.7	−6.7	−5.2	192	4.54	0.002
6. Medial pontomedullary junction	0.9	−6.4	−5.3	110	4.59	0.015
7. Superior colliculus	1.0	−3.5	−1.5	121	3.91	0.011
Region with a significant group difference in metabolic activity						
Mutant > Control						
Cerebellar vermis (lobule VI)§	−0.2	−7.3	−2.7	136	3.26	<0.001‡‖
Correlations between FA and glucose metabolism						
Sensorimotor cortex	3.8	−2.2	−2.0	418	4.10	0.002

*Coordinates according to the common space of SPMMouse (37).
†Cluster size in voxels (1 voxel = 3.4×10^{-4} mm^3).
‡Cluster significant at $P < 0.05$ (Student *t* test), corrected for cluster extent, with additional changes in the contralateral ("mirror") hemisphere.
§According to atlas of Franklin and Paxinos (17).
‖Uncorrected at voxel level.

discrete area within the sensorimotor cortex (Fig. 3*B*, yellow/red). In this gray matter region, metabolic activity exhibited a negative correlation ($P < 0.0005$) with FA values in the superior cerebellar tract (Fig. 3*C*, *Left*). Metabolism in this region also correlated ($P < 0.002$) with the tract abnormality (Fig. 3*C*, *Right*) that was observed in the underlying subcortical white matter (Fig. 3*A*, blue). This correlation was positive, however, and of smaller magnitude than that with the proximal pathway lesion. One interpretation of these findings is that the thalamocortical tract abnormality serves to modulate the increases in sensorimotor cortical activity that, in dystonia gene carriers, have been attributed to reduced cerebellothalamic facilitation of inhibitory cortical interneurons (6, 15, 18, 19).

These observations may also be consistent with the related hypothesis that the distal CbTC tract abnormality mitigates clinical penetrance in nonmanifesting gene carriers by interrupting aberrant signaling at the thalamocortical level (e.g., ref. 15). To explore this possibility, we determined whether the pattern of microstructural change in the mutant animals was consistent with the probabilistic model of gene penetrance that we proposed based on connectivity measurements in human gene carriers (6). Human carriers of autosomal dominant dystonia mutations, whether affected or not, exhibited abnormally reduced FA values proximally in cerebellothalamic projections ($P < 0.001$, post-hoc tests). By contrast, the integrity of the distal thalamocortical segment was significantly lower in the nonmanifesting mutation carriers relative to their affected counterparts ($P < 0.005$) as well as healthy control subjects ($P < 0.0001$). Given that heterozygous *Tor1a*$^{\Delta E/+}$ knock-in mice do not display abnormal movements (16), these animals would be expected to exhibit a substantial distal tract abnormality akin to that observed in the human nonmanifesting carriers. As noted earlier, highly significant FA reductions ($P < 0.0001$) involving both the proximal and distal segments of the CbTC pathway (clusters 1 and 2) were consistently present in the mutant animals. Moreover, the relationship of FA values in these two regions (Fig. 4*B*) was similar to that observed in nonmanifesting human subjects. That is, the reduction in tract integrity was greater in the distal segment relative to the proximal segment of the pathway ($P < 0.002$, paired Student *t* tests). Indeed, this relationship was evident at the individual animal level (see lines connecting the individual data points in Fig. 4*B*). That is, the *Tor1a*$^{\Delta E/+}$ mice, without exception, exhibited lower FA values distally, as was also the case in the human nonmanifesting carriers.

Discussion

We found that *Tor1a*$^{\Delta E/+}$ mice exhibited microstructural abnormalities in cerebellothalamic and thalamocortical pathways, and that these abnormalities correlated with local metabolic activity measured downstream in the sensorimotor cortex. These abnormalities resembled those previously identified in nonpenetrant human mutation carriers who, like the *Tor1a*$^{\Delta E/+}$ mice, do not exhibit abnormal involuntary movements (6). *Tor1a*$^{\Delta E/+}$ mice also exhibit increased metabolic activity in the dorsal cerebellar vermis, a finding consistently identified in manifesting and nonmanifesting human DYT1 carriers (7, 9) and in experimental rodent models of dystonia (20–22). The similarity of these findings indicate that DYT1 mutant torsinA can produce similar CNS changes in mice and humans, and suggest that *Tor1a*$^{\Delta E/+}$ mice are a model of human nonmanifesting DYT1 mutation carriers.

The *Tor1a*$^{\Delta E/+}$ knock-in mice also exhibited significant FA reduction in the caudate/putamen, along with a corresponding deficit in the number of visualized thalamostriatal tracts. Alterations in this tract may affect the regulation of neurotransmitter release in the striatum of these animals (23) and may also relate to the alterations in striatal synaptic plasticity that have recently been observed in a transgenic mouse model with overexpression of the human mutant protein (24). Interestingly, the thalamostriatal tract abnormality failed to reach significance in our earlier study (6) of pathway integrity in human dystonia mutation carriers. The striking deficits in this pathway that were observed in the mouse are attributable to the genetic homogeneity of the sample combined with high-field ex vivo imaging. Together, these features permit the detection of regional changes that may not be easily discerned in the corresponding human studies.

In this vein, the current approach allowed for the detection of tract reductions in projections from the pontine reticular nuclei to the cerebellum in the mutant animals. These small brainstem structures receive afferents from the subthalamic nucleus (25) and have been proposed as conduits of basal ganglia output

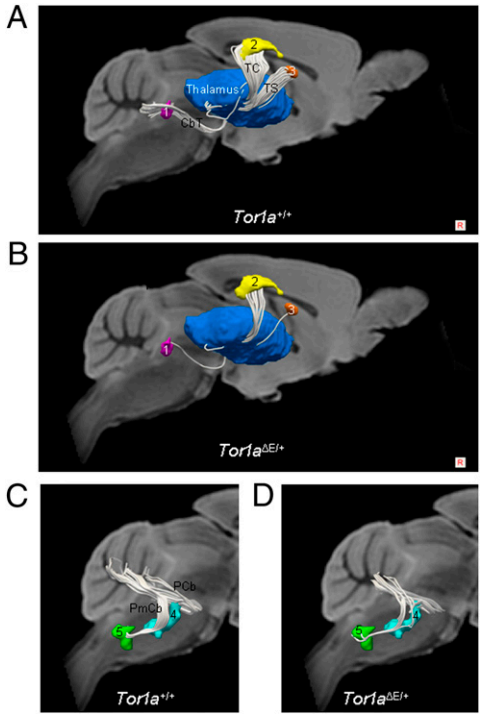

Fig. 2. Connections of the abnormal mutation-related regions visualized by using group tractography. (*A* and *B*) Cerebellothalamic (CbT), thalamocortical (TC), and thalamostriatal (TS) pathways reconstructed in the normal and mutant groups (*Materials and Methods*). In all three pathways, fewer tracts were visualized in the mutant group relative to the controls. (The thalamic seed volume used for fiber tracking is displayed in blue. For clarity, we displayed only 5% of the tracts in the CbT and TC pathways and 15% of tracts in the TS pathway.) (*C* and *D*) Tracts connecting the abnormal pontine and pontomedullary regions with the cerebellum (PCb and PmCb) are also displayed for the two groups. Fewer tracts were also observed in these pathways in the mutant group. P, pontine; Pm, pontomedullary; Cb, cerebellum.

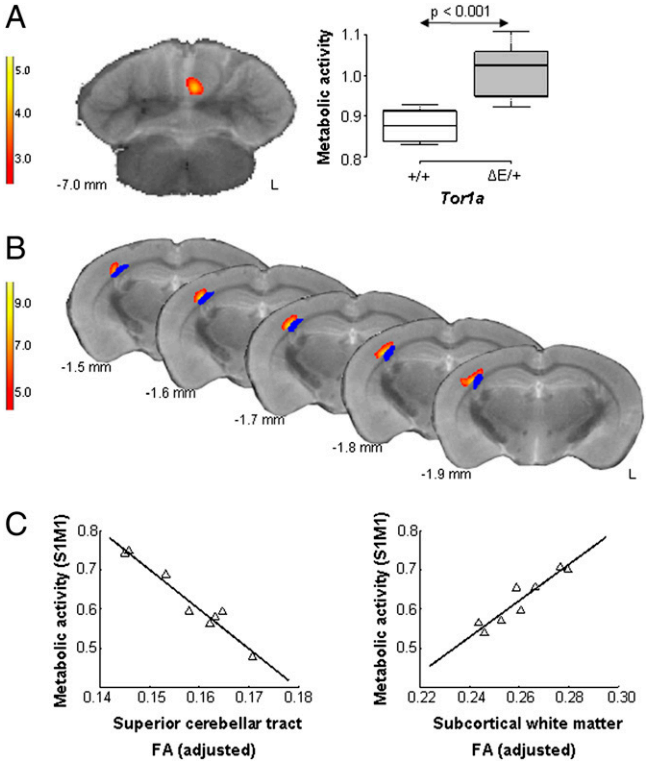

Fig. 3. Metabolic abnormalities and structure–function correlations in the mutant animals. (*A*) An abnormal increase in regional metabolic activity ($P < 0.001$, Student *t* test) was detected in the dorsal cerebellar vermis of the mutant mice (Table 1). The color scale represents *t* values thresholded at 3.4 corresponding to $P = 0.003$ (uncorrected). Individual values for this cluster in the mutant and control animals are represented by box-and-whisker plots. (*B*) Voxel-wise multiple regression analysis revealed a significant correlation between regional metabolic activity in the right sensorimotor cortex (S1M1) and FA values from the superior cerebellar and subcortical white matter clusters, corresponding to the proximal and distal segments of the CbTC pathway. This gray matter region (yellow/red) was found to be situated in close proximity to the distal pathway abnormality (blue). The color scale represents *t* values thresholded at 5.89 corresponding to $P < 0.001$ (uncorrected). (*C*) Multiple regression analysis was performed to examine the relationship between metabolic activity in this cortical region (y) and FA values from the proximal (x_1) and distal (x_2) pathway segments of the mutant animals. This analysis revealed a significant relationship between these measures ($P < 0.0001$, multiple linear regression), which was expressed by the following equation: $y = ax_1 + bx_2 + c$, where $a = -10.02$ ($P = 0.0002$), $b = 4.60$ ($P = 0.0017$), and $c = 1.01$ ($P = 0.0034$). The contributions of each of the abnormal white matter clusters to regional metabolic activity are displayed by leverage plots (42).

signals to the cerebellum. A similar "bridging" function has been suggested for elements of the superior colliculus (26), which also exhibited a significant microstructural abnormality in the mutant animals. Similarly, the microstructural changes identified at the pontomedullary junction are compatible with loss of fiber pathways coursing between the cerebellum and the inferior olivary nucleus. The latter structure is also thought to serve as an interface between the CbTC and basal ganglia/thalamocortical motor networks (27, 28). We note that the significant reductions in tract number observed in the individual DTI clusters can be interpreted as genotype-related abnormalities in the integrity of the respective projection pathways. Nonetheless, these image-derived measures do not necessarily reflect the actual number of fibers coursing within a given white matter bundle. Quantitative studies are needed to compare direct histological indices of tract size and integrity with the corresponding imaging descriptors.

Mice heterozygous for the ΔE mutation in the endogenous torsinA allele have been found to be behaviorally similar to littermate controls, with no discernible motor phenotype (16). Despite the absence of abnormal movements, the mutant animals exhibited changes in regional brain function analogous to those observed in human DYT1 carriers. Metabolic activity was found to be focally increased in the dorsal cerebellar vermis, which connects via the thalamus to cortical motor areas. Interestingly, cerebellar hypermetabolism has been described consistently in manifesting and nonmanifesting human DYT1 carriers (7, 9) and in a genetic rat model of dystonia (20). The observed increase in cerebellar metabolic activity may also reflect a compensatory phenomenon (29).

Along these lines, a hypothesis-testing correlational analysis revealed that individual differences in the integrity of cerebellar projection pathways in the *Tor1a*$^{\Delta E/+}$ mice correlated with metabolic activity measured in the primary motor and sensory cortical regions of these animals. This structure–function relationship corresponded closely to that reported previously in human DYT1 carriers undergoing probabilistic tractography with cerebral blood flow determinations (6). Resting glucose metabolism in the sensorimotor cortex can be viewed as a function of synaptic activity and the balance of local excitation and inhibition (30, 31). In this region, the presence of a positive correlation between metabolism and the integrity of subjacent thalamocortical projections is consistent with a genotype-related attenuation of tract numbers with concomitant reductions in

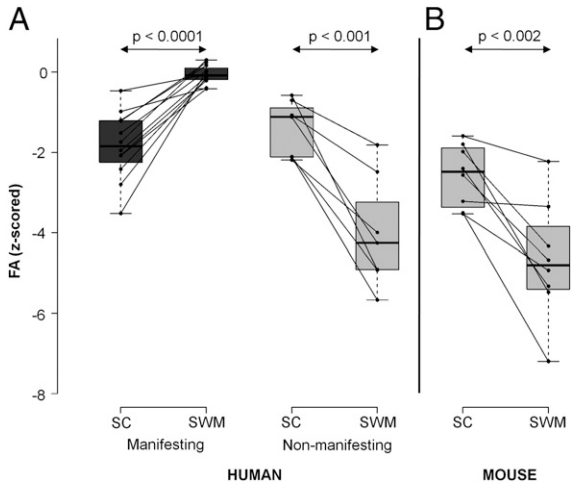

Fig. 4. Regional differences in pathway microstructure: mechanism of penetrance. (*A*) FA measured in the superior cerebellar (SC) pathway and in the subcortical white matter (SWM) subjacent to primary sensorimotor cortex from the previously described cohort of 12 clinically manifesting (MAN) and eight nonmanifesting (NM) dystonia mutation carriers (6). For each region, individual subject FA values were z-transformed with respect to the corresponding cluster values from eight age-matched normal control subjects. Each of the two groups of gene carriers exhibited significant FA reductions in CER relative to controls ($P < 0.001$). By contrast, FA values in SMC were normal in MAN but lower than control values in NM gene carriers ($P < 0.0001$, Student *t* test). (*B*) Plot of z-transformed FA values measured in the homologous regions of the *Tor1a*$^{\Delta E/+}$ mouse. As in human nonmanifesting gene carriers, the mutant animals exhibited significant FA reductions relative to controls ($P < 0.0001$, Student *t* test) in the distal segment of the CbTC pathway in the subcortical white matter.

afferent synaptic activity. That FA values measured in cerebellar outflow pathways were found to correlate negatively with sensorimotor metabolic activity is consistent with the hypothesized role of the ascending CbTC system in facilitating intracortical inhibition via thalamocortical projections to inhibitory interneurons in the sensorimotor cortex (18, 19). In this regard, more severe involvement of the proximal (i.e., cerebellothalamic) pathway segment in mutant animals was associated with relatively greater loss of local cortical inhibition and corresponding increases in regional neural activity (15). In this vein, the additional presence of microstructural abnormalities in the distal (i.e., thalamocortical) pathway segment may serve to modulate the size of the mutation-related functional changes that occur at the cortical level.

Despite significant microstructural alterations in cerebellar pathways, the mutant mice did not exhibit abnormal motor behavior (16). In this regard, these animals resembled human nonmanifesting DYT1 carriers, who also do not develop signs of dystonia during their lifespan (5). In fact, the current data suggest that every heterozygous knock-in animal exhibited a tandem tract deficit at the distal end of the pathway, which served to reduce the likelihood of clinical penetrance. As in the human nonmanifesting carriers, this "second lesion" was of sufficient magnitude to interrupt the abnormal signaling generated proximally by the deficit in cerebellothalamic connectivity. The reason for the consistent presence of a clinically mitigating second lesion in the *Tor1a*$^{\Delta E/+}$ knock-in mice, as opposed to the partial penetrance observed in the human, is not known. Nonetheless, we have observed substantially tighter correlations between connectivity values for the two CbTC segments in the normal mouse relative to the healthy human subjects ($r = 0.9$ and $r = 0.5$, respectively; Pearson correlation coefficients). Indeed, simulations based on the probabilistic connectivity model that we have proposed suggest that "hard wiring" of the circuit during development, as appears to be the case in the rodent, is associated with very low penetrance rates (figure 5C in ref. 6).

Whether the distal pathway abnormality is relatively less pronounced in mutant animals displaying a motor phenotype, similar to clinically manifesting dystonia gene carriers (6), is not currently known. Further studies comparing the current tractographic findings with those from experimental models with observable manifestations will be needed to address this issue. Nonetheless, the presence of consistent microstructural changes in the mutant animals, even if not overtly penetrant, can be regarded as a valuable endophenotype of the disease process. The multimodal animal imaging approach described in the present study can also be used to elucidate the biochemical mechanism of the DYT1 mutation during neurodevelopment. Thus, the findings in the *Tor1a*$^{\Delta E/+}$ knock-in mice can be compared directly with heterozygous mice carrying the analogous KO mutation (*Tor1a*$^{+/-}$). The presence of similar pathway changes in both groups of animals would suggest that the mutant torsinA protein is associated with a loss of function. By contrast, if significant changes in these pathways prove to be present only in the knock-in animals, the gain of an abnormal function becomes a more likely pathogenetic mechanism. In this vein, performing serial microPET and DTI studies in living mutant and control animals, as well as ex vivo tractographic assessments in animals of varying age, will provide valuable information regarding the developmental time course of these system-specific changes (32). Needless to say, it will be of great interest to determine whether similar structure–function abnormalities are discerned by this approach in other experimental models of brain disease.

Materials and Methods

Data Acquisition. Eight C57Bl6/J congenic heterozygous ΔE *Tor1a* knock-in mice (*Tor1a*$^{\Delta E/+}$) and six WT littermate control (*Tor1a*$^{+/+}$) animals were studied at 18 wk of age. These mice were confirmed as fully congenic at Charles River Labs through the use of a panel of genotyping probes. *Tor1a*$^{\Delta E/+}$ and *Tor1a*$^{+/+}$ mice were housed together from birth to assure that all animals experienced as identical an environment as possible. The animals were anesthetized by using ketamine (150 mg/kg) and xylazine (15 mg/kg) and scanned for 15 min on a Siemens Focus 220 microPET instrument, beginning 60 min after the injection of approximately 310 μCi FDG. The resulting images were reconstructed using an iterative algorithm (33, 34) to a matrix size of 128 × 128 × 95 (voxel size, 0.600 mm × 0.600 mm × 0.796 mm).

Following FDG microPET, the animals underwent transcardiac perfusion with 4% paraformaldehyde (35); the brains were harvested and stored in 4% paraformaldehyde for at least 2 wk. Magnetic resonance DTI was performed ex vivo on whole brain samples using the 9.4-T animal magnetic resonance scanner at Johns Hopkins Medical Center (36). Diffusion weighted images of these specimens were acquired by using a rapid acquisition with relaxation enhancement sequence in six directions with a maximum b-value of 2,138 s/mm^2. Two additional images with a b-value of 210 s/mm^2 were also acquired. Each acquisition included six echoes with two repetitions to improve the signal-to-noise ratio. The DTI data acquisition matrix was 136 × 84 × 64, which was zero-filled before Fourier transformation to 272 × 168 × 128. The field of view was 17 mm × 10.5 mm × 8 mm. The nominal resolution of the DTI images was 62.5 μm × 62.5 μm × 62.5 μm, with a total ex vivo imaging time of approximately 20 h. Institutional animal care and use committees at Johns Hopkins University School of Medicine and Weill Medical College of Cornell University approved all animal procedures.

Data Analysis. After DTI data acquisition, maps of FA were calculated, as well as the entire diffusion tensor for tractography. A nine-parameter affine registration was applied to the individual animal FA maps by using FSL software (http://www.fmrib.ox.ac.uk/fsl/). When they had been aligned, the FA images were smoothed by using a kernel of 312.5 μm (full width at half maximum) and the two groups were compared voxel-wise over the entire brain volume by using SPMMouse software (http://www.wbic.cam.ac.uk/~sjs80/spmmouse.html), a new toolbox for statistical parametric mapping in the mouse (37). Group differences were considered significant at a voxel-level threshold of $P = 0.001$ with a correction for multiple comparisons at

$P < 0.05$. We also reported regional differences at a hypothesis testing threshold of $P < 0.001$ (voxel level uncorrected) with a cluster cutoff of 100 voxels. The individual data from the resulting clusters were measured post hoc. Values for the mutant and control groups were displayed graphically by using box-and-whisker plots to evaluate overlapping data and potential outlier effects. Each significant cluster within a given hemisphere was transposed to the opposite side and measured for the two groups. FA values for each significant cluster, on each hemisphere separately, were compared across groups by using Student *t* tests and were considered significant at $P < 0.05$.

Following the identification of discrete regions with significant FA abnormalities in the mutant animals, white matter pathways passing through these areas were reconstructed separately for the two groups. Tractography was performed on the images from each group using an early registration method by which the DTI scans were registered to a common template before tensor calculation (38). We used TrackVis software (http://www.trackvis.org/) to map white matter pathways coursing between volumes of interest delineated in the mutant and control animals; tracking parameters were identical for the two groups. The resulting tracts were verified using AKILLIDTI software (39), which uses a different tractography algorithm (40). In this study, the significant clusters identified by voxel-based comparison of the FA maps for the two groups were used as seed volumes for tractography. Mean tracts were displayed for each group and compared qualitatively based on visualized tract size.

For quantitative comparison of the two groups, tractographic analysis was also performed in the native space of each animal. The significant clusters identified in standard space were reverse-transformed, and fiber tracking was then performed on each sample individually. To account for fixation-dependent FA differences between specimens, tracking parameters were adjusted by using the FA histogram peaks as reference for the individual samples. Fiber counts were conducted for each reconstructed tract in every animal. Mean values for the mutant and control groups were compared by using Student *t* tests; group differences were considered significant for *P* values lower than 0.05.

The microPET data were analyzed by using a similar approach to that described for the DTI group comparisons. Individual images were registered to a standard template (41) by using an iterative algorithm. Group differences in regional metabolic activity were assessed on a voxel basis with SPMMouse; the threshold for significance was the same as for the voxel-based comparison of the FA maps. We also tested the hypothesis that, as in human DYT1 carriers (6), functional activity at the major nodes of the CbTC network is correlated with individual differences in the microstructural integrity of this pathway. This possibility was examined by conducting a voxel-wise multiple regression analysis in SPMMouse, and the results were considered significant at a voxel-level threshold of $P = 0.001$ with a correction for multiple comparisons at $P < 0.05$. The contribution of each FA regressor to metabolic activity in the significant brain regions was evaluated post-hoc by using leverage plot analysis (42) in JMP software (SAS Institute). These correlations were considered significant at $P < 0.05$.

ACKNOWLEDGMENTS. We thank Drs. S. Vallabhajosula and J. Dyke and Dr. S. Mori for their assistance with the imaging procedures, and Ms. Toni Fitzpatrick for assisting in manuscript preparation.

1. Tanabe LM, Kim CE, Alagem N, Dauer WT (2009) Primary dystonia: Molecules and mechanisms. *Nat Rev Neurol* 5:598–609.
2. Breakefield XO, et al. (2008) The pathophysiological basis of dystonias. *Nat Rev Neurosci* 9:222–234.
3. Ozelius LJ, et al. (1997) The early-onset torsion dystonia gene (DYT1) encodes an ATP-binding protein. *Nat Genet* 17:40–48.
4. Risch N, et al. (1995) Genetic analysis of idiopathic torsion dystonia in Ashkenazi Jews and their recent descent from a small founder population. *Nat Genet* 9:152–159.
5. Bressman SB, et al. (2000) The DYT1 phenotype and guidelines for diagnostic testing. *Neurology* 54:1746–1752.
6. Argyelan M, et al. (2009) Cerebellothalamocortical connectivity regulates penetrance in dystonia. *J Neurosci* 29:9740–9747.
7. Carbon M, Eidelberg D (2009) Abnormal structure-function relationships in hereditary dystonia. *Neuroscience* 164:220–229.
8. Eidelberg D, et al. (1998) Functional brain networks in DYT1 dystonia. *Ann Neurol* 44: 303–312.
9. Trošt M, et al. (2002) Primary dystonia: is abnormal functional brain architecture linked to genotype? *Ann Neurol* 52:853–856.
10. Hutchinson M, et al. (2000) The metabolic topography of essential blepharospasm: A focal dystonia with general implications. *Neurology* 55:673–677.
11. Carbon M, et al. (2004) Regional metabolism in primary torsion dystonia: Effects of penetrance and genotype. *Neurology* 62:1384–1390.
12. Carbon M, et al. (2004) Microstructural white matter changes in carriers of the DYT1 gene mutation. *Ann Neurol* 56:283–286.
13. Carbon M, Kingsley PB, Tang C, Bressman S, Eidelberg D (2008) Microstructural white matter changes in primary torsion dystonia. *Mov Disord* 23:234–239.
14. Sanes JN, Donoghue JP (2000) Plasticity and primary motor cortex. *Annu Rev Neurosci* 23:393–415.
15. Carbon M, et al. (2010) Increased sensorimotor network activity in DYT1 dystonia: a functional imaging study. *Brain* 133:690–700.
16. Goodchild RE, Kim CE, Dauer WT (2005) Loss of the dystonia-associated protein torsinA selectively disrupts the neuronal nuclear envelope. *Neuron* 48:923–932.
17. Franklin KBJ, Paxinos G (2007) *The Mouse Brain in Stereotaxic Coordinates* (Academic Press, New York), 3rd Ed.
18. Daskalakis ZJ, et al. (2004) Exploring the connectivity between the cerebellum and motor cortex in humans. *J Physiol* 557:689–700.
19. Molinari M, Filippini V, Leggio MG (2002) Neuronal plasticity of interrelated cerebellar and cortical networks. *Neuroscience* 111:863–870.
20. Brown LL, Lorden JF (1989) Regional cerebral glucose utilization reveals widespread abnormalities in the motor system of the rat mutant dystonic. *J Neurosci* 9:4033–4041.
21. Neychev VK, Fan X, Mitev VI, Hess EJ, Jinnah HA (2008) The basal ganglia and cerebellum interact in the expression of dystonic movement. *Brain* 131:2499–2509.
22. Pizoli CE, Jinnah HA, Billingsley ML, Hess EJ (2002) Abnormal cerebellar signaling induces dystonia in mice. *J Neurosci* 22:7825–7833.
23. Smith Y, et al. (2009) The thalamostriatal systems: Anatomical and functional organization in normal and parkinsonian states. *Brain Res Bull* 78:60–68.
24. Martella G, et al. (2009) Impairment of bidirectional synaptic plasticity in the striatum of a mouse model of DYT1 dystonia: Role of endogenous acetylcholine. *Brain* 132: 2336–2349.
25. Bostan AC, Dum RP, Strick PL (2010) The basal ganglia communicate with the cerebellum. *Proc Natl Acad Sci USA* 107:8452–8456.
26. May PJ (2006) The mammalian superior colliculus: Laminar structure and connections. *Prog Brain Res* 151:321–378.
27. Marshall SP, Lang EJ (2004) Inferior olive oscillations gate transmission of motor cortical activity to the cerebellum. *J Neurosci* 24:11356–11367.
28. LeDoux MS, Lorden JF (2002) Abnormal spontaneous and harmaline-stimulated Purkinje cell activity in the awake genetically dystonic rat. *Exp Brain Res* 145:457–467.
29. Carbon M, et al. (2008) Increased cerebellar activation during sequence learning in DYT1 carriers: An equiperformance study. *Brain* 131:146–154.
30. Sokoloff L (1999) Energetics of functional activation in neural tissues. *Neurochem Res* 24:321–329.
31. Sibson NR, et al. (1998) Stoichiometric coupling of brain glucose metabolism and glutamatergic neuronal activity. *Proc Natl Acad Sci USA* 95:316–321.
32. Xiao J, Gong S, Zhao Y, LeDoux MS (2004) Developmental expression of rat torsinA transcript and protein. *Brain Res Dev Brain Res* 152:47–60.
33. Nuyts J, Fessler JA (2003) A penalized-likelihood image reconstruction method for emission tomography, compared to postsmoothed maximum-likelihood with matched spatial resolution. *IEEE Trans Med Imaging* 22:1042–1052.
34. Mirrione MM, et al. (2007) A novel approach for imaging brain-behavior relationships in mice reveals unexpected metabolic patterns during seizures in the absence of tissue plasminogen activator. *Neuroimage* 38:34–42.
35. Mori S, et al. (2001) Diffusion tensor imaging of the developing mouse brain. *Magn Reson Med* 46:18–23.
36. Zhang J, et al. (2005) Magnetic resonance diffusion tensor microimaging reveals a role for Bcl-x in brain development and homeostasis. *J Neurosci* 25:1881–1888.
37. Sawiak SJ, Wood NI, Williams GB, Morton AJ, Carpenter TA (2009) Voxel-based morphometry in the R6/2 transgenic mouse reveals differences between genotypes not seen with manual 2D morphometry. *Neurobiol Dis* 33:20–27.
38. Ulug AM, Vo A, Argyelan M, Eidelberg D (2009) Early registration of diffusion tensor images for group tractography. *Magn Reson Mater Phys Biol Med* 22(suppl 1):107.
39. Demir A, Firat Z, Ozkan M, Ulug AM (2009) Brain white matter visualization tool (AKILLIDTI). *Magn Reson Mater Phys Biol Med* 22 (suppl 1):540.
40. Watts R, Liston C, Niogi S, Ulug± AM (2003) Fiber tracking using magnetic resonance diffusion tensor imaging and its applications to human brain development. *Ment Retard Dev Disabil Res Rev* 9:168–177.
41. Ma Y, et al. (2005) A three-dimensional digital atlas database of the adult C57BL/6J mouse brain by magnetic resonance microscopy. *Neuroscience* 135:1203–1215.
42. Sall J (1990) Leverage plots for general linear hypothesis. *Am Stat* 44:308–315.